This is an author's version published in: **http://oatao.univ-toulouse.fr/23917**

To cite this version:

Any correspondence concerning this service should be sent to the repository administrator: tech-oatao@listes-diff.inp-toulouse.fr

Performance of chromia- and alumina-forming Fe- and Ni-base alloys exposed to metal dusting environments: The effect of water vapor and temperature

Aurelie Rouaix-Vande Put [a,*], Kinga A. Unocic [b], Michael P. Brady [b], Bruce A. Pint [b]

[a] Université de Toulouse, Institut Carnot CIRIMAT, INPT-ENSIACET, 4 allée Emile Monso, CS 44362, 31030 Toulouse Cedex 4, France
[b] Materials Science & Technology Division, Oak Ridge National Laboratory, 1 Bethel Valley Road, 37831 Oak Ridge, TN, USA

A B S T R A C T

Fe and Ni base alloys including an alumina forming austenitic alloy were exposed for 500 h under metal dusting environments with varying temperature, gas composition and total pressure. For one H_2 CO CO_2 H_2O environment, the increase in temperature from 550 to 750 °C generally decreased metal dusting. When H_2O was added to a H_2 CO CO_2 environment at 650 °C, the metal dusting attack was reduced. Even after 5000 h at a total pressure of 9.1 atm with 20%H_2O, the higher alloyed specimens retained a thin protective oxide. For gas mixtures containing little or no H_2O, the Fe base alloys were less resistant to metal dusting than Ni base alloys.

1. Introduction

Metal dusting is a catastrophic form of corrosion occurring between 400 and 800 °C in environments for which the carbon activity (a_c) is greater than 1. It leads to the disintegration of metallic materials as a result of the formation of a carbon deposit containing metallic particles, carbides and oxides. A large number of studies have been devoted to define which alloys and composi tions [1 8] are more resistant to metal dusting. The influence of alloy grain size [3,9], surface finish, cold working [3,9 12] or the addition of a coating [13 16] on the resistance to such corrosion has been evaluated. Other studies were interested in the effect of parameters defining the metal dusting environment: temperature [12,17], total pressure [11,17 19] or gas composition [19 23].

Quantifying degradation by metal dusting is complex because there is no single gas mixture, temperature and total pressure encountered in industrial applications. Those parameters differ with the application and process, which results in a wide range of laboratory studies and difficulties comparing experimental results. One relevant observation about laboratory studies is that typical gas compositions creating a metal dusting environment contain little or no water vapor, in general <10% and very few contain ⩾20% of H_2O. However, Hoffman et al. [24] reported that industrial applications can contain up to 40% H_2O, in addition to being run at a high total pressure. These differences between laboratory and industrial conditions appeared to be significant as laboratory studies tend to highlight the superiority of Ni base alloys, as shown by Grabke et al. [25], while Hoffman et al. [24] reported better resistance for Fe base alloys under industrial conditions.

This study surveyed the influence on metal dusting of temper ature as well as H_2O content and total pressure (expanding initial results published previously [26,27]). Three sets of tests were defined. The first one was carried out at atmospheric pressure in a given CO_2 CO H_2 H_2O mixture with the temperature being raised from 550 to 750 °C. The second one was carried out at 650 °C and atmospheric pressure in a CO_2 CO H_2 environment in which H_2 was replaced by H_2O, leading to a decrease in a_c. The third one was also performed at 650 °C under the same CO_2 CO H_2 environment in which H_2O was added from 0 to 28% by keeping the CO/CO_2 and CO/H_2 ratios constant and raising the total pressure to keep a_c constant. Under each metal dusting environ ment, a wide range of commercial chromia and alumina forming Fe and Ni base alloys were tested. The test matrix also included a new class of alumina forming austenitic (AFA) stainless steels, alloys developed at Oak Ridge National Laboratory to offer both good oxidation and creep resistance [28 30]. Select alloys were also oxidized at 650 °C in wet air to compare the effect of water vapor in high and low oxygen partial pressures.

* Corresponding author.
E-mail addresses: aurelie.rouaix@ensiacet.fr (A. Rouaix-Vande Put), unocicka@ornl.gov (K.A. Unocic), bradymp@ornl.gov (M.P. Brady), pintba@ornl.gov (B.A. Pint).

2. Experimental procedure

2.1. Materials

A series of chromia and alumina forming Fe and Ni base alloys was studied under metal dusting conditions. Their chemical composition is given in atomic percent in Table 1. The alloy spec imens were rectangular coupons (typically $\approx 1.5 \times 10 \times 19$ mm), except for 3 mm thick H224 specimens, or 16 mm diameter disks for cast FeCrAlY and NiAl. A hole was drilled close to one end to facilitate their positioning within the rig. Samples were ground to a 600 grit finish with SiC paper on all faces and then cleaned ultrasonically in acetone and methanol before being exposed to metal dusting/oxidizing environments for 500 h. After an ultra sonic cleaning of the samples in acetone to remove coke, post test mass changes were measured using a Mettler Toledo model XP205 balance (±0.02 mg accuracy).

2.2. Metal dusting exposures

In order to study the effect of temperature and H_2O content on the metal dusting resistance of alloys, 9 metal dusting conditions were designed. They were defined using the gas mixture, the temperature, the carbon activity (a_c) and the oxygen partial pressure (P_{O_2}). The carbon activity can be calculated using:

(a) the synthesis gas reaction : $H_2 + CO \quad H_2O + C$

$$a_c \quad \frac{K_1 \times P_{CO} \times P_{H_2}}{P_{H_2O}} \tag{1}$$

(b) the Boudouard reaction : $2CO \quad CO_2 + C$

$$a_c \quad \frac{K_2 \times P_{CO}^2}{P_{CO_2}} \tag{2}$$

(c) the hydrocarbon cracking reaction : $CH_4 \quad 2H_2 + C$

$$a_c \quad \frac{K_3 \times P_{CH_4}}{P_{H_2}^2} \tag{3}$$

where K_i are the equilibrium constants of the corresponding reac tions and P_i the partial pressures of CO, CO_2, H_2 and H_2O.

The carbon activity of a CO_2 CO H_2 H_2O gas mixture can then be calculated using either the synthesis gas reaction or the Boudouard reaction. As the synthesis gas reaction is faster than the Boudouard reaction [31,32], a_c is commonly determined using reaction (1). The oxygen partial pressure P_{O_2} is calculated using the following reaction:

$$H_2O \quad H_2 + 1/2O_2 \quad P_{O_2} \quad \left(\frac{K_4 \times P_{H_2O}}{P_{H_2}} \right)^2 \tag{4}$$

In the case of a CO_2 CO H_2 environment without H_2O, a_c cannot be determined using reaction (1) but rather with reaction (2) and P_{O_2} is calculated using reaction (5):

$$CO_2 \quad CO + 1/2O_2 \quad P_{O_2} \quad \left(\frac{K_5 \times P_{CO_2}}{P_{CO}} \right)^2 \tag{5}$$

Those 9 metal dusting environments were organized in three sets:

(1) At atmospheric pressure, for a 59%H_2 35%CO 2%CO_2 4%H_2O gas mixture, the temperature was increased from 550 to 750 °C, leading to a decrease in a_c from 69.4 to 1.4 (Tests 1 3 in Table 2).
(2) At atmospheric pressure and 650 °C, a_c was decreased from 10 to 1.1 by replacing H_2 by H_2O in a 43%CO 51%H_2 6%CO_2 gas mixture (Tests 4 6 in Table 2).
(3) At 650 °C, H_2O was added to a 43%CO 51%H_2 6%CO_2 gas mixture keeping the CO/CO_2 and H_2/CO ratios constant. The total pressure was increased from 1 to 16 atm in order to maintain a_c around 10 (Tests 4' and 7 9 in Table 2). Metal dusting conditions in Test 4 and 4' were identical and compared exposures in the two furnaces described below.

Adding up to 20%H_2O to a 43%CO 51%H_2 6%CO_2 environment at atmospheric pressure leads to a large decrease in a_c that rapidly becomes inferior to 1. To maintain conditions favorable to metal dusting, i.e. a_c greater than 1, CO and CO_2 contents were kept con stant and H_2 was replaced by H_2O in the second set of experiments. However, degradation by metal dusting is dependent on the ratio between H_2 and CO, as shown by Zhang et al. [20] on iron exposed at 700 °C to various H_2 CO 0.19 vol%H_2O environments. To isolate the effect of H_2O, CO/CO_2 and H_2/CO ratios were kept constant in

Table 1
Composition of the alloys in at%.

Alloy	Fe-base alloys					Ni-base alloys					
	T122	800H	347H	AFA	FeCrAlY	601	602	693	HR6W	H224	NiAl
Fe	84.74	42.72	68.19	48.42	70.14	12.84	9.27	4.70	24.41	26.74	
Ni	0.33	31.84	7.89	23.63		58.45	58.05	57.70	44.38	42.92	52.46
Cr	11.36	20.90	19.87	14.69	20.01	23.74	26.22	29.99	26.28	21.12	
Al		1.43		7.08	9.77	2.66	4.80	6.23	0.09	7.20	47.53
Si	0.24	0.55	2.20	0.29		0.46	0.16	0.10	0.44	0.48	
Co	0.02	0.06	0.12			0.05	0.03	0.04	0.44	0.24	
Cu	0.73	0.30	0.22	0.43		0.48	0.01	0.01	0.09	0.01	
Mn	0.68	0.99	0.95	1.94		0.21	0.10	0.19	1.04	0.34	
Mo	0.21	0.10	0.17	1.15		0.21	0.02	0.02	0.1	0.14	
Nb	0.02	0.04	0.02	1.47		0.06	0.01	0.37	0.12		
V	0.24	0.05	0.03	0.05		0.05	0.03		0.06	0.02	
Ti		0.60		0.06		0.55	0.17	0.47	0.17	0.54	
W	0.57	0.01	0.01	0.30			0.003		1.99		
Others	0.01B	0.02P	0.004B	0.03B	0.07Y	0.02B	0.04B	0.01P	0.02B	0.0001Y	
	0.02P	0.01Zn	0.03P	0.03P		0.02P	0.06Y	0.03Zr	0.02P		
							0.06Zr				
C	0.51	0.36	0.21	0.42	0.004	0.13	0.86	0.12	0.32	0.23	
S	<0.3	<0.09	0.006	<0.00003	<0.03	0.005	<0.3	$<9 \times 10^{6}$	<0.3	0	$<9 \times 10^{6}$
O	0.012	0.004	0.011	0.003	0.007	0.003	0.100	0	0.013	0.005	0.002
N	0.297	0.026	0.093	0.002	0.0004	0.060	0.002	0.04	0.028	0.015	0

Test	T (°C)	P_{total} (atm)	Gas mixture (%)				a_c	P_{O_2} (atm)
			H_2O	CO	H_2	CO_2		
1	550						69.4	9.7×10^{29}
2	650	1.0	4.0	35.0	59.0	2.0	8.1	2.4×10^{25}
3	750						1.4	1.3×10^{22}
4			0		51.0		10.0	2.4×10^{25}
5	650	1.0	10	43.0	41.0	6.0	2.8	3.1×10^{24}
6			20		31.0		1.1	2.2×10^{23}
4'		1.0	0	43.0	51.0	6.0	10.0	2.4×10^{25}
7	650	3.6	10	38.7	45.9	5.4	10.0	2.5×10^{24}
8		9.1	20	34.4	40.8	4.8	10.0	1.3×10^{23}
9		16.0	28	31.0	36.7	4.3	10.2	3.1×10^{23}
Ox	650	1.0	Air + 10%H_2O				–	0.21

the third set of experiments. In this set, the decrease in a_c due to the addition of H_2O was compensated by an increase in total pressure. Then, the increase in total pressure will have to be taken into account in the discussion on the H_2O effect.

The calculation of a_c and P_{O_2} was performed using the "reaction" module of Factsage version 6.1 software. These metal dusting conditions are represented according to their carbon activity and oxygen partial pressure in Fig. 1a.

An isothermal oxidation for 500 h at 650 °C in air + 10%H_2O at 1 atm (Test 'Ox' in Table 2) was also carried out on select alloys to study their behavior with water vapor and a high oxygen partial pressure.

Tests Ox and 1–6 were conducted in a horizontal alumina tube in a resistively heated furnace with the specimens hung on alumina rods resting on the sides of an alumina boat, Fig. 1b. The samples were positioned so that their faces were parallel to the gas flow. For Tests 5 (10%H_2O, a_c = 2.76) and Ox, the specimens were sitting in the alumina boat and did not have a hole. The gas flow rate was 300 cc/min for the H_2O free gas mixture. It was decreased for Tests 2–3 and 5–6 in order to account for the water vapor addition, made by atomizing filtered, deionized and deaerated water (≈0.065 μS/cm conductivity) into the flowing gas. The gas mixture was created from three separate gas cylinders of H_2, CO and CO_2. For Tests 4' and 7–9, a resistively heated furnace enclosed a vertical 9 cm diameter × 92 cm long tube made of alloy 230 and a stainless steel flange at the top. The specimens were attached to a slotted

alumina tube using Pt wire, Fig. 1c. The gas mixing system was similar to that of the horizontal furnace, except that the 43CO–51H_2–6CO_2 gas mixture was premixed. The gas flow rate was also fixed at 300 cc/min in the case of the H_2O free environment. Because of slightly different internal diameter between tubes, gas velocities are in the same order of magnitude at atmospheric pressure (5.4 cm/min and 4.7 cm/min for respectively the furnace working at 1 atm and the one able to maintain high total pressures).

2.3. Characterization

After exposure, the surface of some specimens was analyzed by X-ray diffraction (XRD) using a PANalytical X'Pert Pro diffractometer with Cu Kα radiation (45 kV/40 mA) with a 2° incidence angle. Morphology was examined by scanning electron microscopy (SEM) using a Hitachi model S4800. In the case of cross section characterization, specimens were Cu plated, sectioned and metallography polished.

3. Results

3.1. Effect of the temperature

The mass changes from Tests 1–3 at 550–750 °C are reported in Fig. 2. At 550 °C with the highest a_c, all of the Fe base alloys lost mass (347H was not included), and three Ni base alloys (601, H224, NiAl) exhibited mass losses. The largest mass losses were encountered for T122 and 800H alloys, which exhibited the largest visual surface degradation, while some degradation around the hole was responsible for the mass loss of the AFA alloy. The mass loss of H224 alloy was associated with the formation of many little pits, while no attack was observed associated with the very small mass loss for the NiAl specimen (−0.002 mg/cm²).

When the temperature was increased to 650 °C, only two Fe base alloys lost mass: 347H and T122. The mass loss of the T122 specimen was smaller at 650 °C than at 550 °C. At 750 °C, a mass gain was recorded for the T122 specimen. The decrease in the degradation of T122 alloy with increasing temperature and decreasing a_c is illustrated with cross sections in Fig. 3. The pits decreased in size from 550 to 650 °C and, at 750 °C, an apparently continuous oxide scale formed, Fig. 3c. Based on SEM–EDS analysis, the oxide scale contained mainly Cr and Mn.
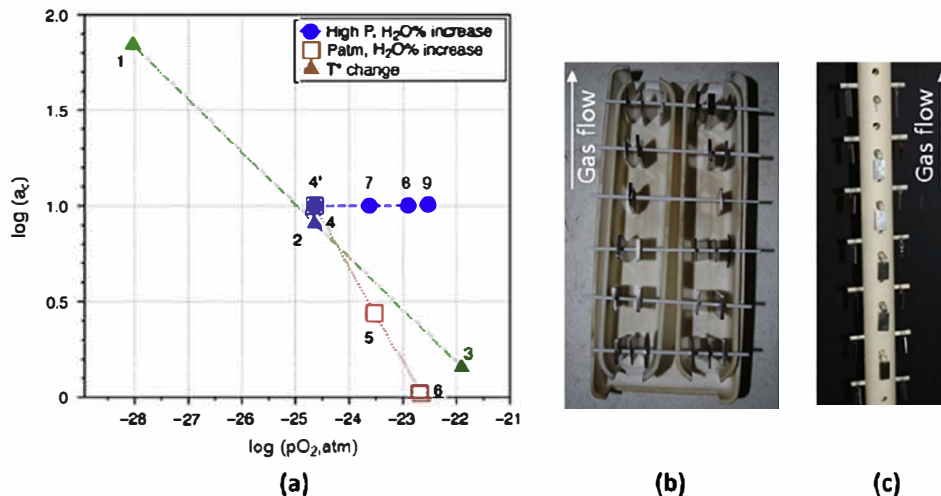

Fig. 1. (a) Diagram representing a_c versus P_{O_2} of the metal dusting environments. Sample arrangement (b) in Tests 1–6, at atmospheric pressure and (c) in Tests 4' and 7–9, at a total pressure from 1 atm to 16 atm.
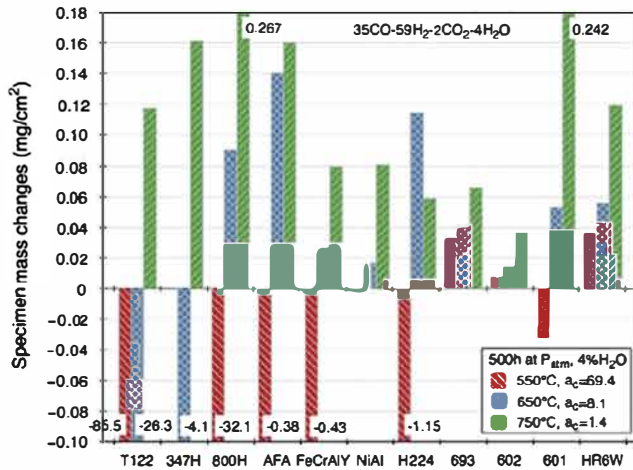
Fig. 2. Mass changes after exposure in a 35%CO–59%H$_2$–2%CO$_2$–4%H$_2$O gas mixture for 500 h and P_{atm} for Tests 1 (550 °C, a_c = 69.4), 2 (650 °C, a_c = 8.1), 3 (750 °C, a_c = 1.4).

Fig. 4. Mass changes after exposure in a (51–X)%H$_2$–43%CO–6%CO$_2$–X%H$_2$O gas mixture for 500 h at 650 °C and P_{atm} for Tests 4 (0%H$_2$O, a_c = 10), 5 (10%H$_2$O, a_c = 2.76) and 6 (20%H$_2$O, a_c = 1.05). When duplicate specimens were tested, the average mass change is reported and error bars indicate the exact mass changes.

3.2. Decrease in a_c by replacing H$_2$ with H$_2$O, at 1 atm

The mass changes from Tests 4 6 at 650 °C with varying H$_2$/H$_2$O ratios are shown in Fig. 4. Mass losses were only observed after Test 4 without H$_2$O, where five alloys exhibited mass losses: Ni base alloy 601 and four Fe base alloys with T122 having the greatest mass loss. With the addition of water vapor in Tests 5 and 6 all of the specimens exhibited small mass gains with no clear trends with the increase in H$_2$O between these two experiments except for T122, which showed the highest mass gain in Test 6. A small mass gain was measured for alloy H224 specimen after Test 4 despite two pits visible on its surface. This will be discussed elsewhere [33].

Pictures of selected specimens from Tests 4 6 are shown in Fig. 5. Consistent with the mass losses in Test 4, significant degradation was visible for the T122, 347H, 800H and AFA specimens with large and numerous pits observed on T122, 347H and AFA, Fig. 6. Pits were observed on the edges of 800H alloy (Fig. 6c) and small pits on the alloy 601 specimen, Fig. 6e. The benefit of adding H$_2$O in Tests 5 and 6 also is clear in Fig. 5 where no pitting was observed. After Test 5, SEM characterization of the T122 specimen surface confirmed the absence of pits, Fig. 7a and b. However, areas exhibiting a dark contrast were visible. According to EDS analysis, they were C rich, suggesting an attack by metal dusting. After Test 6, the T122 surface did not show any sign of metal dusting attack, Fig. 7c e. However, the oxide scale that developed exhibited two microstructures typical of outward growing oxides that would not be expected for oxidation of T122 in air, Fig. 7d and e. Based on EDS analyses, the large oxides on the T122 surface were Fe rich, Fig. 7d, while the whiskers type oxides were rich in Cr, Fe and Mn, Fig. 7e.

Fig. 8 shows polished cross sections of the T122 and AFA specimens after Tests 4 and 5. Consistent with the observations above, significant pitting 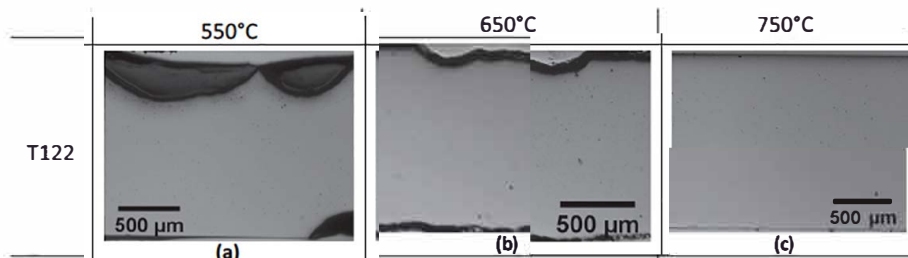occurred for both alloys after Test 4 but not with the addition of H$_2$O in Test 5. This difference could be attributed to the lower a_c with the addition of H$_2$O, thus the final set of experiments was conducted with a_c held constant by increasing the pressure.

3.3. Constant a_c = 10 with increasing H$_2$O% and total pressure

The specimen mass changes for Tests 4' and 7 9 are reported in Fig. 9. When duplicate specimens were exposed, the average is shown and one standard deviation noted. Similar to Tests 4 6, mass losses were only encountered in Test 4' without H$_2$O. Similar to the results for Test 4, mass losses were observed for T122 and 347H due to pit formation. However, the other Fe base alloys showed mass gains and only H224 exhibited a mass loss. No specific degradation was observed to justify the small mass loss for the H224 specimen. The specimen could have been damaged while removing the Pt Rh wire, which was blocked by deposits. Two AFA specimens were exposed in Test 4' and both exhibited minor pitting but not sufficient to result in a mass loss as in Test 4. Small pits also were observed for the T122, 601 and HR6W specimens. For Tests 7 9 containing increasing water vapor contents and increasing pressure, the mass gains were typically small with no particular trend. One exception was the NiAl specimens exposed to 20% and 28%H$_2$O. Very high mass gains were observed for these specimens, which was surprising given previous reports of excellent metal dusting resistance [8]. The NiAl behavior will be discussed elsewhere [33].

Fig. 10 shows the surface morphology of the T122 specimens in these four experiments. In addition to the large pits observed after Test 4', the surface of T122 exhibited C rich areas, appearing with a dark contrast in Fig. 10a. With the addition of H$_2$O, Fe rich oxide nodules formed, Fig. 10b and c, which is consistent with the large

Fig. 3. Light optical microscopy of T122 cross-sections after 500 h of exposure in a 59%H$_2$–35%CO–2%CO$_2$–4%H$_2$O environment at atmospheric pressure and at (a) 550 °C (a_c = 69.4), (b) 650 °C (a_c = 8.1), (c) 750 °C (a_c = 1.4).
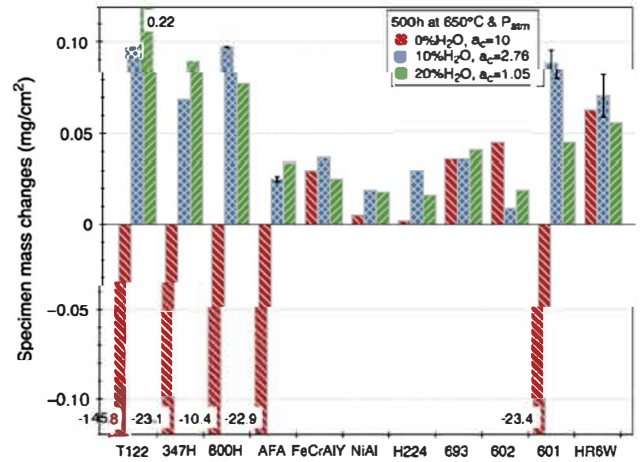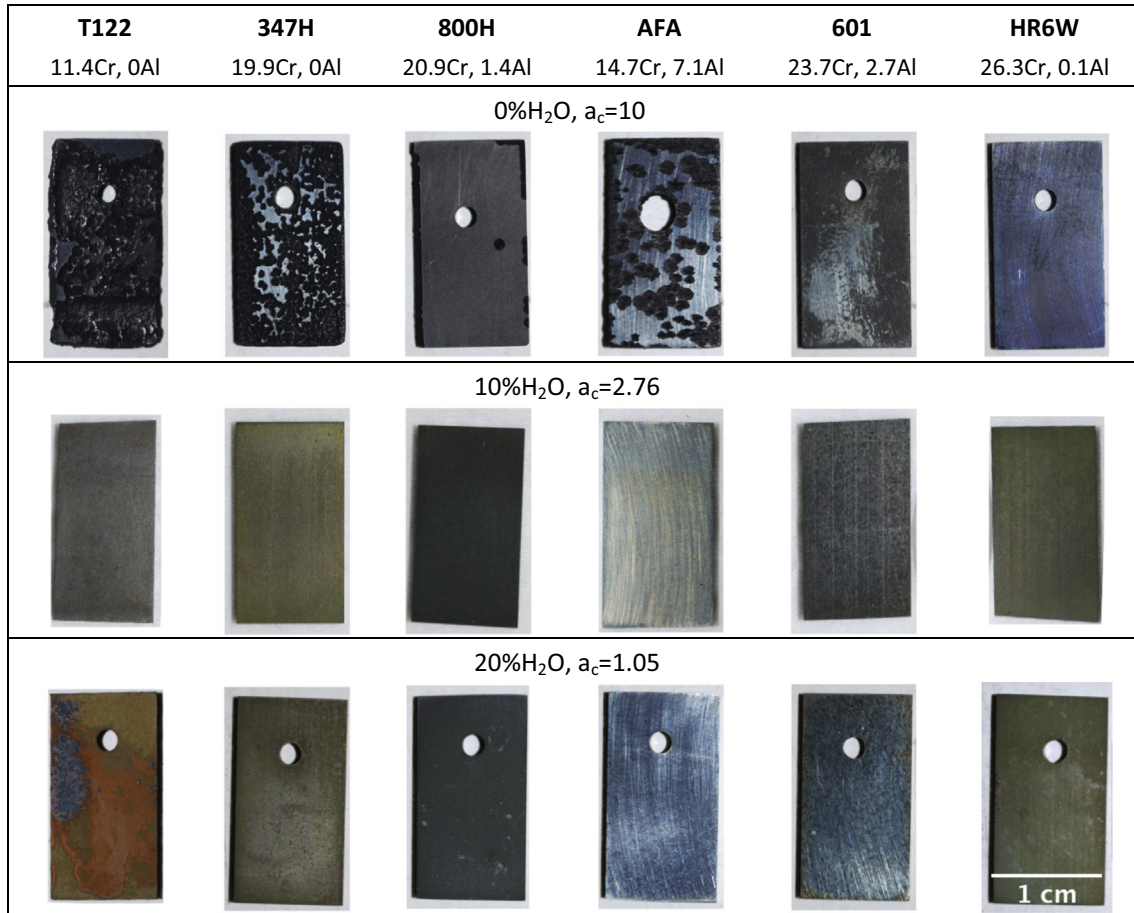
T122	347H	800H	AFA	601	HR6W
11.4Cr, 0Al	19.9Cr, 0Al	20.9Cr, 1.4Al	14.7Cr, 7.1Al	23.7Cr, 2.7Al	26.3Cr, 0.1Al

0%H$_2$O, a$_c$=10

10%H$_2$O, a$_c$=2.76

20%H$_2$O, a$_c$=1.05

1 cm

Fig. 5. Samples after exposure for 500 h at 650 °C and P_{atm} in a (51–X)%H$_2$–43%CO–6%CO$_2$–X%H$_2$O gas mixture for Tests 4 (0%H$_2$O, a_c = 10), 5 (10%H$_2$O, a_c = 2.76) and 6 (20%H$_2$O, a_c = 1.05). Cr and Al concentrations are given in at%.

(a) T122   **(b)** 347H   **(c)** 800H

(d) AFA   **(e)** 601
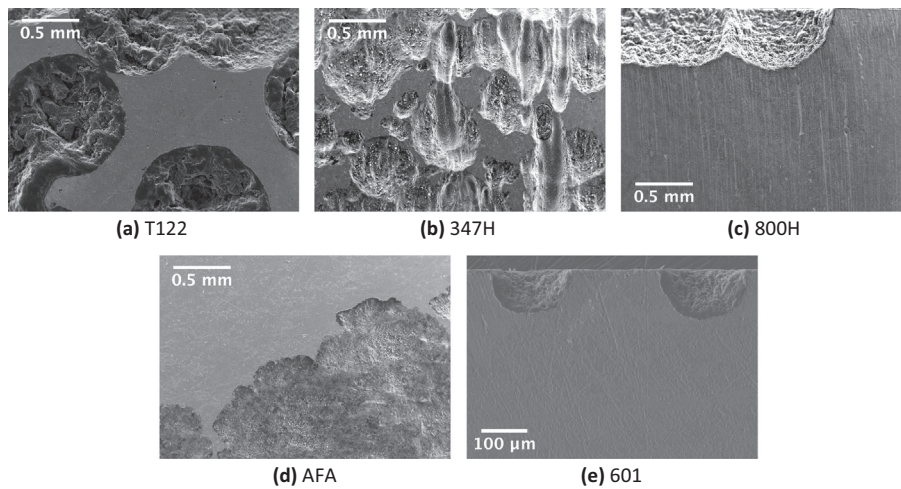
Fig. 6. SEM images of the surface of (a) T122, (b) 347H, (c) 800H, (d) AFA and (e) 601 alloys after Test 4 (500 h at 650 °C and P_{atm}, 51%H$_2$–43%CO–6%CO$_2$, a_c = 10). SE mode.

mass gains measured. The nodules were concentrated on one end of the sample with 10%H$_2$O, while they were uniformly distributed over the entire surface with 20%H$_2$O in Test 8. After Test 9, the T122 surface appeared uniformly oxidized without nodules, Fig. 10d, which is consistent with the smaller mass gain measured (compared to Tests 7 and 8). XRD analysis of these specimens detected spinel and FeO for Test 8 but spinel and Cr$_2$O$_3$ oxides after exposure in the other environments, Fig. 11.

In order to investigate long term performance, Test 8 was continued for 5000 h (10 × 500 h cycles). The specimen mass change data versus time is shown in Fig. 12. Since the T122 and NiAl specimens exhibited high mass gains after 500 h, they were not continued for longer times. For the other specimens, the mass changes after 5000 h remained small and positive, and a thin oxide scale formed on the surface that did not exhibit any sign of metal dusting attack, examples are shown in Fig. 13.
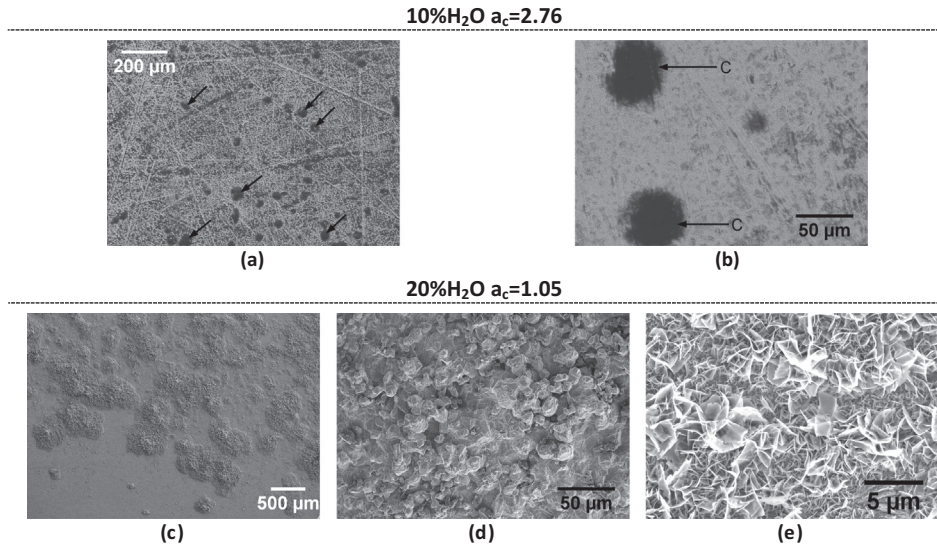
Fig. 7. SEM images of the surface of T122 alloy after 500 h at 650 °C and P_{atm} in a (51–X)%H_2–43%CO–6%CO_2–X%H_2O gas mixture for (a and b) Test 5 (10%H_2O, a_c = 2.76) and (c–e) Test 6 (20%H_2O, a_c = 1.05). Image (b) is a high magnification of (a), (d) and (e) are respectively high magnification images of nodules and the flat surface observed on image (c). SE mode.
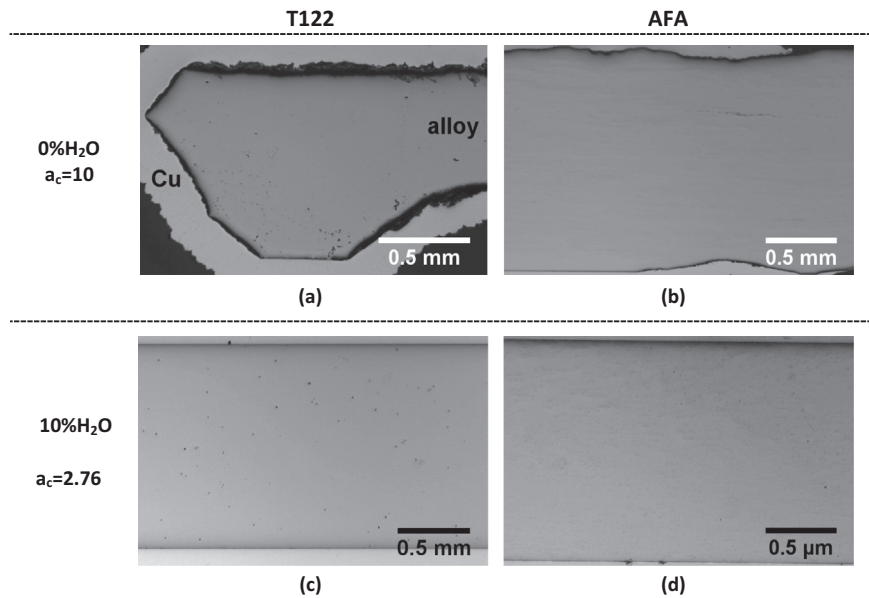

Fig. 8. Optical images of T122 and AFA cross-sections after exposure in a (51–X)%H_2–43%CO–6%CO_2–X%H_2O gas mixture at 650 °C and P_{atm} for (a–b) Test 4 (0%H_2O, a_c = 10) and for (c–d) Test 5 (10%H_2O, a_c = 2.76).

3.4. Oxidation compared to metal dusting

Because of the high mass gains and FeO_x nodule formation observed in some cases with the addition of water vapor, a final experiment was conducted with air + 10%H_2O and compared with the results from Test 5 in Fig. 14. The T122 specimen exhibited a much larger mass gain after the wet air test than after the metal dusting test. In contrast, the 347H, 800H, HR6W and 602 alloys exhibited mass losses during the oxidation, which was not observed in Test 5, perhaps due to the lower P_{O_2}. The large mass gain for the T122 specimen and large mass loss for the 347H specimen are both typical of accelerated attack (i.e. FeO_x formation) in the presence of wet air where the thick Fe rich oxide remains adherent to the ferritic martensitic steel and spalls from the austenitic steel due to its larger thermal expansion mismatch with the oxide [34]. The remaining oxides on T122 and 347H are

shown in Fig. 15a and b. In Fig. 15b, only the Cr rich inner scale is present, the outer Fe rich oxide had spalled. Also, the accelerated attack was not uniform on the 347H specimen, perhaps because part of the specimen was shielded by the alumina boat. Surprisingly, small mass losses were also observed from the 800H and HR6W specimens. It is possible this is related to evaporation of $CrO_2(OH)_2$ due to the presence of O_2 and H_2O [35]. The AFA alloy formed a protective and stable oxide scale, Fig. 15c.

4. Discussion

4.1. Effect of the temperature

The decrease in metal dusting degradation observed with the increase in the temperature from 550 to 750 °C is consistent with
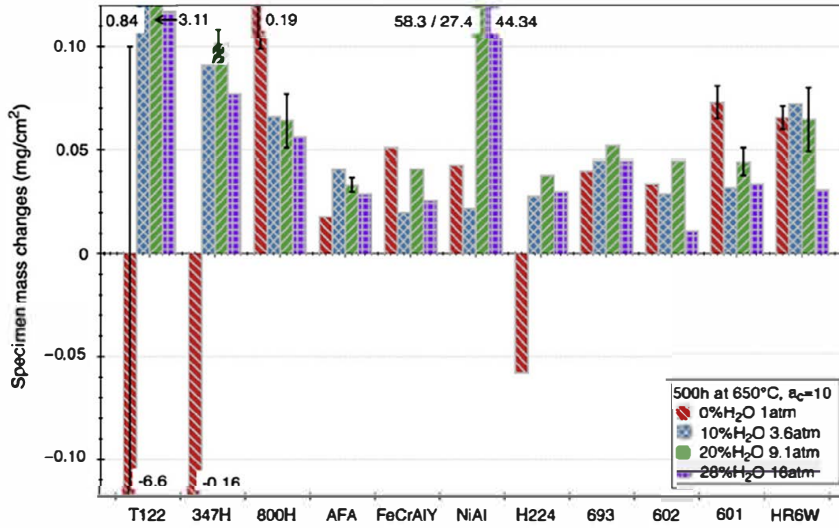
Fig. 9. Mass changes after exposure in a H_2–CO–CO_2–H_2O gas mixture (with H_2/CO = 1.2 and CO/CO_2 = 7.2) for 500 h at 650 °C and a_c = 10 for Tests 4' (0%H_2O, 1 atm), 7 (10%H_2O, 3.6 atm), 8 (20%H_2O, 9.1 atm) and 9 (28%H_2O, 16 atm). When duplicate specimens were tested, the average mass change is reported and error bars indicate the mass change of each sample. In the case of T122 and NiAl, the given numbers are real mass changes, not an average.
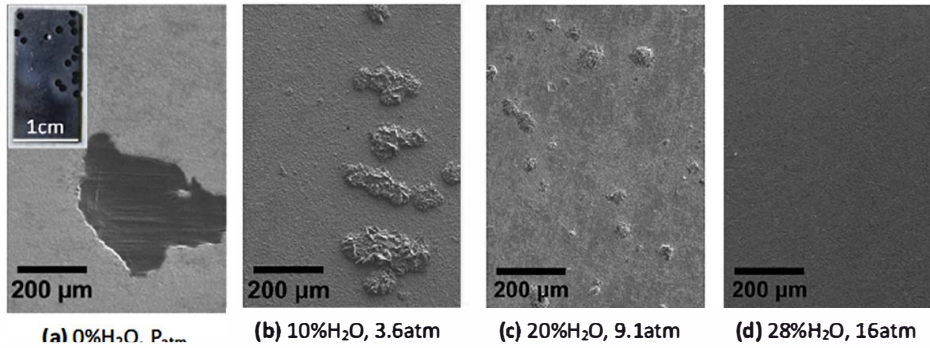

Fig. 10. SEM images of the surface of T122 alloy after exposure in a H_2–CO–CO_2–H_2O gas mixture (with H_2/CO = 1.2 and CO/CO_2 = 7.2, a_c = 10) at 650 °C for 500 h (a) Test 4' (0%H_2O, P_{atm}), (b) Test 7 (10%H_2O, 3.6 atm), (c) Test 8 (20%H_2O, 9.1 atm), (d) Test 9 (28%H_2O, 16 atm).
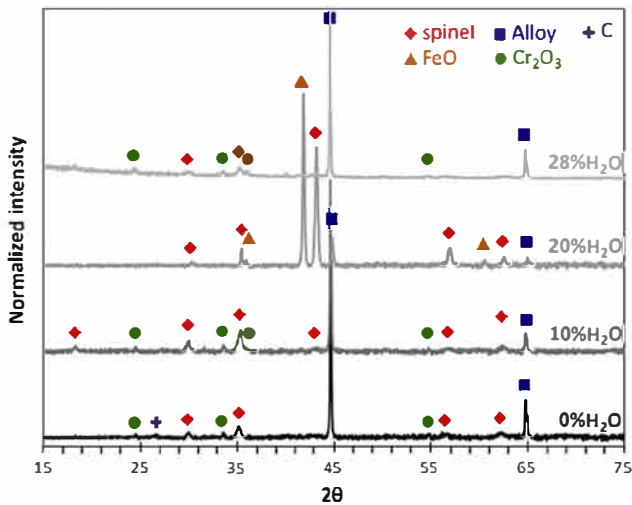

Fig. 11. XRD diagrams obtained by analyzing T122 surface after Tests 4' (0%H_2O, P_{atm}), 7 (10%H_2O, 3.6 atm), 8 (20%H_2O, 9.1 atm) and 9 (28%H_2O, 16 atm) at 650 °C for 500 h and a_c = 10.
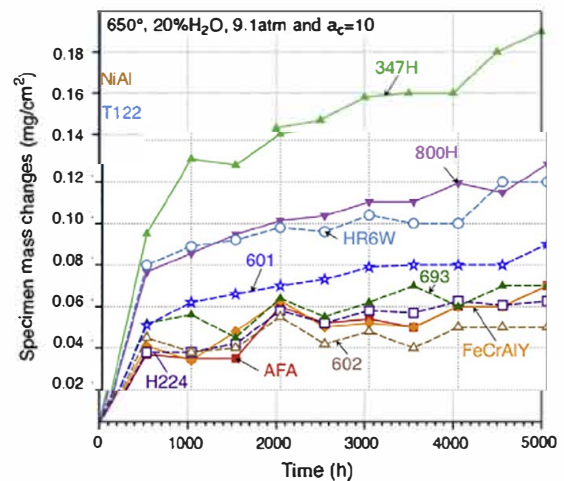

Fig. 12. Mass changes versus time for metal dusting Test 8 (650 °C, 20%H_2O, a_c = 10, 9.1 atm).

the decrease in the equilibrium constant of the synthesis gas reaction [32], leading to a decrease in a_c, Table 2. This is also in agreement with the works of Grabke and Müller Lorenz [3], who

proposed that a temperature below 600 °C favors metal dusting and the study of Chun et al. [36] who observed a maximum metal dusting rate at 575 °C for iron exposed to a 50%CO 50%H_2 environment. However, the temperature at which carbon formation and
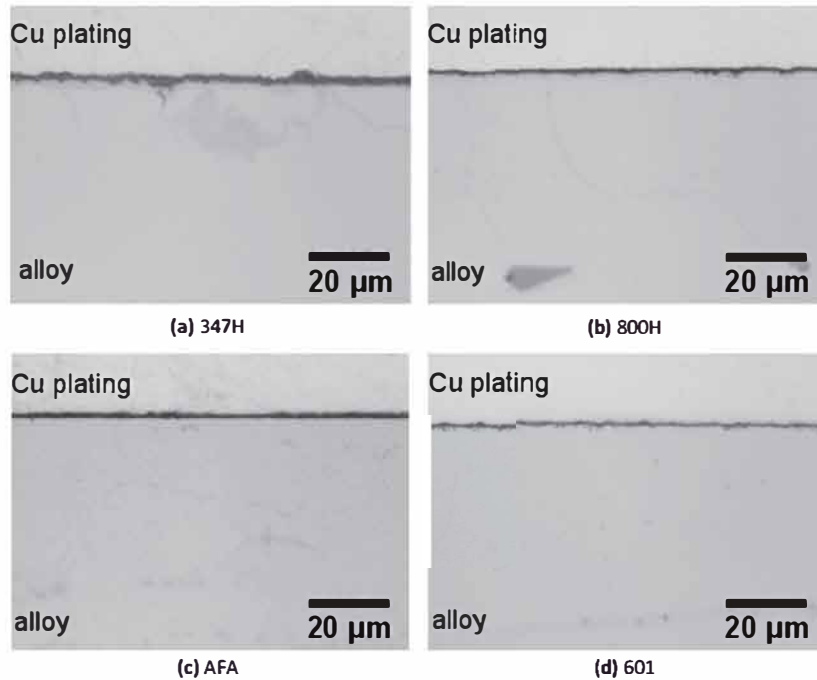
(a) 347H

(b) 800H

(c) AFA

(d) 601

Fig. 13. Light optical microscopy of (a) 347H, (b) 800H, (c) AFA, (d) 601 cross-sections after 5000 h in Test 8 (650 °C, 20%H_2O, a_c = 10, 9.1 atm).
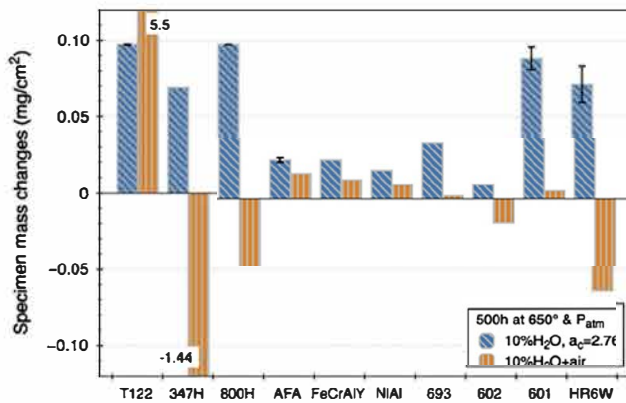

Fig. 14. Mass changes after 500 h of exposure at 650 °C and P_{atm} for the metal dusting Test 5 (10%H_2O, a_c = 2.76) and the oxidizing test in air + 10%H_2O. When duplicate specimens were tested, the average mass change is reported and error bars indicate the exact mass changes.

metal dusting are the strongest depend on the gas mixture composition, the tested materials and the total pressure. In 1959, Walker et al. [37] studied rates of carbon formation on iron catalysts and found that increasing the H_2 content of a CO H_2 mixture increased the temperature at which the maximum rate of carbon deposition

occurred (528 °C for a 0.8%H_2 rich mixture and 630 °C for a 19.9%H_2 mixture). On Ni and alloy 600 specimens, Schneider et al. [38] noticed a maximum carbon uptake rate at 625 °C in a H_2 24%CO 2%H_2O gas mixture. On a 316SS specimen exposed at atmospheric pressure to a 75%H_2 25%CO gas mixture at temperatures ranging from ~450 650 °C, Levi et al. [18] observed a more severe metal dusting attack when the temperature was increased. Under the same gas mixture but at a total pressure of 2 MPa or 3 MPa, they reported a similar trend. Finally, a 800H specimen subjected to a 454 777 °C thermal gradient in a 24%CO 47%H_2 6%CO_2 23%H_2O gas mixture at 4×10^6 Pa under went pitting over the 607 713 °C range while at 2.5×10^6 Pa, the pits were scattered over the 605 676 °C range (with the maximum number of pits reported respectively at 650 660 °C and 610 620 °C) [17]. Based on these last two studies that pointed out a greater degradation under high total pressures for temperatures around 650 °C [17,18], the current series of tests focused on this temperature.

While increasing temperature leads to a decrease in a_c, it also results in faster diffusion, which should favor the establishment of a continuous chromia/alumina layer at higher temperatures. In the case of T122, significant Mn was detected within the oxide scale formed at 750 °C. This is consistent with results for 800H [17] where lower Fe/Mn ratios within the oxide scale were measured after exposures above 700 °C compared to 613 °C.
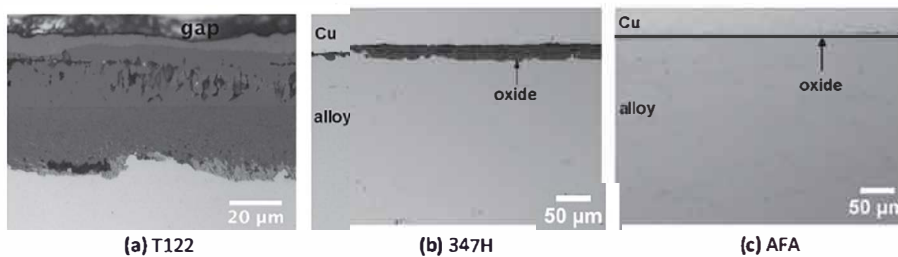

(a) T122

(b) 347H

(c) AFA

Fig. 15. Light optical images of the cross-sections of alloys (a) T122, (b) 347H and (c) AFA after 500 h at 650 °C and P_{atm} after the oxidation test in air + 10%H_2O.

At 550 °C, all the Fe base alloys were attacked (347H was not included) while only two out of six Ni base alloys experienced mass losses (the mixed chromia /alumina forming alloy 601 and alumina forming H224). After exposure at 650 °C, only two Fe base alloys underwent mass losses (T122 and 347H). This confirms the superior behavior of Ni base alloys under metal dusting conditions containing little water vapor. This is also consistent with the works of Toh et al. [39] and Nishiyama et al. [7] who observed a lower resistance to metal dusting for 800 and 601 alloys at respectively 680 °C in a CO 26 vol%H_2 6 vol%H_2O environment and 650 °C in a 60%CO 26%H_2 11.5%CO_2 2.5%H_2O. Toh et al. also noticed a weak resistance of 602CA alloy, which was not observed in this study [39]. However, both studies [7,39] used thermal cycling, which is more aggressive than these results, which were mostly isothermal.

4.2. Decrease in a_c by replacing H_2 by H_2O at 1 atm

The reduction/suppression of degradation by adding H_2O is widely known and has been observed on various alloys [40 42]. According to Hochman [40], such a decrease in the metal dusting attack could be explained by H_2O affecting the alloy oxidation as well as by affecting the O_2 and C activities. Because the addition of H_2O increases the oxygen activity and blocks reactions releasing free C on the surface, the probability of developing sites of "low O_2 activity high C activity", conditions favorable for pitting attack, is decreased [40]. A decrease in the CO dissociation rate due to water adsorption causing a blocking of surface reaction centers has been later confirmed experimentally on a Cr sample [43]. In the present work, the addition of H_2O to the H_2 CO CO_2 gas mixture led to a decrease in a_c and was done by decreasing the H_2 content, Table 2. Grabke [44] showed that H_2 accelerates the transfer of C from CO in the case of iron. Later, the rate of C uptake of pure iron was found to increase when increasing the CO content, up to about 60 75%, at 700 °C in a CO H_2 0.19%H_2O gas mixture [20]. Therefore, the absence of metal dusting observed with the increase in the H_2O content could also be due to the decreases in both the a_c and the H_2 content.

The 500 h exposure at 650 °C, in 51%H_2 43%CO 6%CO_2 (Test 4) led to apparent surface attack by metal dusting of four Fe base alloys (T122, 347H, 800H, AFA) and two Ni base alloys (601 and H224). This is also consistent with the widely reported better behavior of Ni base alloys exposed at atmospheric pressure to metal dusting environments containing little or no H_2O.

4.3. Carbon activity equal to 10 while increasing H_2O% and total pressure

The effect of pressure is not commonly investigated but more severe metal dusting attack has been reported with increasing test pressure [11,17 19]. Contrary to Hochman who explained that low P_{O_2} and a_c sites are favorable for metal dusting [40], Nishiyama et al. [17] considered that an increase in P_{O_2} is harmful because it lowers the oxide scale integrity by creating defects. In their work, for a given gas mixture, an increase in the total pressure favored metal dusting because it increased P_{O_2} in addition to raising a_c [17]. In these experiments, P_{CO} was increased from 0.43 atm to 4.96 atm. Despite that increase, no degradation by metal dusting was noticed with the addition of H_2O, confirming the beneficial effect of H_2O in preventing metal dusting. Because high H_2O contents and high pressures lead to higher P_{O_2}, favoring the formation of an oxide scale, the absence of metal dusting attack could be a matter of incubation time. However, extending Test 8 to 5000 h did not change the results for any of the specimens.

In addition to showing the great impact of the H_2O addition on metal dusting prevention, this set of experiments illustrates that a_c is not the only key criterion to evaluate a possible attack by metal dusting. Instead of considering a_c as a quantification of the environment harmfulness, every parameter constituting the environment has to be taken into account: (i) nature of the gases, (ii) gas content, (iii) total pressure, (iv) P_{O_2} and (v) temperature.

Concerning the T122 behavior, Cr_2O_3 and a spinel oxide were identified as the main constituents of its oxide scale after exposures in atmospheres containing 0%, 10% and 28%H_2O while FeO and a spinel oxide composed the oxide scale formed in the 20%H_2O rich environment. Cr_2O_3 and the spinel oxide are commonly formed under metal dusting conditions. The presence of FeO is unusual but this oxide could form under the higher oxygen partial pressures of Tests 7 9, according to the calculated phase equilibria at 627 °C of the Fe Cr O system [45]. According to EDS and SEM analyses, the nodules observed under 10 and 20%H_2O rich environments are Fe rich, outward and fast growing oxides. They could be FeO oxides. The absence of FeO on the XRD diagram for 10%H_2O is therefore surprising. While those nodules were uniformly distributed on the surface exposed to 20%H_2O, they were mainly concentrated close to one end on the surface exposed to 10%H_2O. Thus the region analyzed by XRD may not have contained nodules. While arguing that there is a sufficiently high oxygen partial pressure and H_2O accelerated oxidation, the absence of Fe rich nodules after exposure to 16 atm and 28%H_2O is therefore surprising. However, it is consistent with the low mass gain, smaller than those obtained after testing in 10% and 20%H_2O and under a high total pressure. In 2008, Essuman et al. observed accelerated internal oxidation for Fe Cr alloys exposed to H_2O containing atmospheres at 900 °C and 1050 °C compared to O_2 rich atmospheres [46]. In the present study, the highest H_2O content associated with the highest total pressure of Test 9 could have modified T122 oxidation behavior by favoring the formation of more stable oxides, therefore hindering nodules formation.

4.4. Effect of the alloy composition

Among the alloys tested in these metal dusting conditions, T122 and 347H are low concentration of Cr alloys containing no Al which likely explains their poor behavior. Increasing Cr and Al contents in 800H, led to more protective behavior. There is likely a synergistic benefit of higher Ni content, as was observed in model Fe Cr Ni alloys in water vapor [47]. For the alumina forming Fe base alloys, FeCrAlY behaved very well except after the exposure at 550 °C (which will be addressed in a future paper [33]). While ferritic FeCrAlY has little creep strength at 650 °C, the AFA alloys were designed to have high creep strength due to their nano carbide precipitates [29,30] as well as good oxidation resistance in air and wet air by the formation of an alumina scale [28,48]. A consequence of this balancing of oxidation resistance and mechanical properties is that austenitic AFA is not as "strong" an alumina former as ferritic FeCrAlY type alloys, perhaps due to slower Al diffusion in austenite. Despite the generally good oxidation behavior of AFA in oxidizing environments at 650° 800 °C, the AFA specimens were attacked in the H_2O free metal dusting environment and after exposure at 550 °C in an atmosphere containing 4%H_2O. Other AFA alloys, with different compositions, were tested at 650 °C in 50%CO 49%H_2 1%H_2O (a_c = 36.7, P_{O_2} = 2.83 × 10 ^{26} atm) under thermal cycling (1 h) conditions by Zhang et al. [49]. While the rates for metal wastage were low for the first 100 cycles, they observed large mass losses after ~350 cycles, suggesting that the protective oxide scale was not durable. The AFA alloy evaluated in this study contained 0.4 at% Cu, 14.7 at% Cr and 7.1 at% Al. It has been shown that Cu additions prevent metal dusting for Ni [4,50], Ni base alloys [51], stainless steels [52] and model Fe Ni Cu alloys [53]. However, these Cu additions are usually higher than that present in AFA, which was added to improve creep strength. The poor behavior of this AFA composition is probably due to

insufficient Al and Cr contents to guarantee the formation of a protective oxide scale under such aggressive conditions. Another concern is that the majority of carbide forming elements in AFA are already linked to carbon, so any carbon ingress during exposure will lead to Cr carbide formation in an alloy with relatively low Cr. It is also possible that the elements added to strengthen AFA, such as Mo and W, may not be beneficial for metal dusting resistance. However, 3%W or 3%Mo additions to Fe 32Ni 20Cr were found to improve metal dusting resistance [2].

Regarding Ni base alloys, 601 and H224 were degraded after exposure at 550 °C. Specimens of 601 and HR6W exhibited tiny pits after Test 4' (650 °C, 0%H_2O, a_c = 10) despite a positive mass change while H224 exhibited a mass loss (probably due to the removing of the Pt Rh wire). Also, alloy 601 was strongly attacked after Test 4 (650 °C, 0%H_2O, a_c = 10) but not HR6W. From these results, alloy HR6W appears to have somewhat better resistance to metal dusting than alloy 601. Alloy HR6W contains 26.3 at% Cr but no Al while 601 has less Cr (23.7 at%) and some Al (2.7 at%): a level not sufficient to form an alumina scale formation but does cause significant internal oxidation, which could disrupt the chro mia scale. However, 500 h exposures are relatively short duration tests and the difference observed between HR6W and 601 could also be a matter of incubation time.

4.5. Effect of the rig/furnace wall material

Tests 4 and 4' with the same temperature and gas conditions were conducted in order to compare the results in two different experimental rigs. In general, there was less pitting attack in Test 4' (Figs. 4 and 9). The different behavior cannot be explained by the number of specimens as more samples were exposed in Test 4. The other differences between the tests were the sample arrangement within the rigs, the reaction tubes and the gas cylin ders. The specimens were placed in a horizontal alumina tube for Test 4. Test 4' was performed using a vertical pre oxidized alloy 230 tube. While the gas mixture inlet and exhaust were placed at opposite ends of the horizontal alumina tube, both inlet and exhaust were located at the top of the alloy 230 tube and the inlet gas flowed through a FeCrAl (Kanthal AF) tube to the bottom and then the gas flowed up across the specimens. It is possible that some reaction occurred within this FeCrAl tube or with the alloy 230 tube, leading to a change in the gas mixture composition (less carburizing) and therefore to a lower attack. In addition, one gas cylinder containing the appropriate gas mixture was used for Test 4' while three separate cylinders were used to create the gas mixture of Test 4. Despite the fact that all those cylinders con tained high purity gases, the impurities present in the gas mixture were probably not exactly the same between both tests. Different oxygen impurities would affect P_{O_2} while sulfur impurities would inhibit metal dusting [32,54].

5. Conclusions

A series of chromia and alumina forming Fe and Ni base alloys were exposed under nine different metal dusting and one air + H_2O environments. For a given gas mixture composition, increasing the temperature from 550 to 750 °C at atmospheric pressure reduced the a_c, leading to reduced metal dusting attack, as expected. At 650 °C and atmospheric pressure, the replacement of H_2 by H_2O in a CO H_2 CO_2 environment also reduced a_c and led to reduced alloy degradation. At 650 °C, the addition of H_2O to a CO H_2 CO_2 gas mixture in association with an increase in the total pressure to maintain a_c equal to 10 also prevented metal dusting attack. One condition with 20%H_2O and 9.1 atm was continued for 5000 h to determine if the oxides would break down after longer exposures. However, among the alloys that were protective at 500 h, none showed degradation by metal dusting during the longer exposure. Both of these sets of experiments illustrate the beneficial effect of water vapor, which is commonly used in industrial applications. As has been found in many studies, atmo spheric pressure, high a_c environments containing little or no H_2O cause severe attack of Fe base alloys compared to Ni base alloys. However, the differences among Fe and Ni base alloys with similar Cr and/or Al levels were reduced in metal dusting environ ments containing H_2O. The experiments at constant a_c indicate that the beneficial effect of H_2O is not simply related to increasing the oxygen partial pressure and reducing a_c. For low alloyed steels such as T122, the beneficial effect of H_2O was not the same as for higher alloyed materials. While H_2O did prevent pitting in T122, the presence of H_2O generally led to thick, Fe rich oxide formation in high a_c environment, similar to that observed in air + H_2O.

References

[1] H.J. Grabke, E.M. Müller-Lorenz, B. Eltester, M. Lucas, D. Monceau, Resistance of 9–20%Cr-steels against metal dusting, Steel Res. 68 (1997) 179–185.

[2] S. Strauβ, H.J. Grabke, Role of alloying elements in steels on metal dusting, Mater. Corros. 49 (1998) 321–327.

[3] H.J. Grabke, E.M. Müller-Lorenz, Protection of high alloy steels against metal dusting by oxide scales, Mater. Corros. 49 (1998) 317–320.

[4] J. Zhang, D.M.I. Cole, D.J. Young, Alloying with copper to reduce metal dusting of nickel, Mater. Corros. 56 (2005) 756–764.

[5] Y. Nishiyama, N. Otsuka, T. Kudo, Metal dusting behaviour of Cr–Ni steels and Ni-base alloys in a simulated synga mixture, Corros. Sci. 48 (2006) 2064–2083.

[6] J. Zhang, D.J. Young, Coking and dusting of Fe–Ni alloys in CO–H_2–H_2O gas mixtures, Oxid. Met. 70 (2008) 189–211.

[7] Y. Nishiyama, N. Otsuka, S. Matsumoto, H. Matsuo, Metal Dusting Behaviour of New Ni-base Alloy in a Laboratory Carbonaceous Environment, in: Paper Presented at the Conference NACE Corrosion, Atlanta (GA), USA, March 22–26, 2009.

[8] P. Speck, D.J. Young, J. Zhang, Metal dusting of nickel–aluminium alloys, Oxid. Met. 73 (2010) 255–274.

[9] H.J. Grabke, E.M. Müller-Lorenz, S. Strauss, E. Pippel, J. Woltersdorf, Effects of grain size, cold working, and surface finish on the metal-dusting resistance of steels, Oxid. Met. 50 (1998) 241–254.

[10] D. Monceau, E.M. Müller-Lorenz, H.J. Grabke, Metald dusting resistance of steels, Mater. Sci. For. 251–254 (1997) 665–670.

[11] M. Maier, J.F. Norton, P.D. Frampton, Metal dusting of 9–20%Cr steels in increased pressure environments at 560 °C, Mater. Corros. 49 (1998) 330–335.

[12] C.M. Chun, T.A. Ramanarayanan, Metal dusting corrosion of austenitic 304 stainless steel, J. Electrochem. Soc. 152 (2005) B169–B177.

[13] C. Rosado, M. Schütze, Protective behaviour of newly developed coatings against metal dusting, Mater. Corros. 54 (2003) 831–853.

[14] C.M. Chun, T.A. Ramanarayanan, Metal dusting resistant alumina forming coatings for syngas production, Corros. Sci. 51 (2009) 2770–2776.

[15] A. Agüero, M. Gutierrez, L. Korcakova, T.T.M. Nguyen, B. Hinnemann, S. Saadi, Metal dusting protective coatings. A literature review, Oxid. Met. 76 (2011) 23–42.

[16] C. Geers, M. Schütze, Behavior of Nickel–Tin Coated High Temperature Materials Exposed Under Metal Dusting Conditions, in: Paper Presented at the Conference NACE Corrosion, Houston (TX), USA March 13–17, 2011.

[17] Y. Nishiyama, K. Kitamura, N. Otsuka, Metal dusting behaviour of alloy 800H in laboratory carbonaceous environments under high pressure, Mater. Sci. For. 595–598 (2008) 649–660.

[18] T.P. Levi, N. Briggs, I.E. Minchington, C.W. Thomas, Metal dusting of type 316 stainless steel in high pressure environments between 450 °C and 650 °C, Mater. Corros. 53 (2002) 239–246.

[19] K. Natesan, Z. Zen, Development of Materials Resistant to Metal Dusting Degradation, Technical Report ANL-06/14, Argonne National Laboratory (IL), USA, 2007.

[20] J. Zhang, A. Schneider, G. Inden, Effect of gas composition on cementite decomposition and coke formation on iron, Corros. Sci. 45 (2003) 281–299.

[21] Y. Nishiyama, T. Kudo, N. Otsuka, Effect of syngas composition on metal dusting of alloy 800H in simulated reforming gas atmospheres, Corrosion 62 (2006) 54–63.

[22] A. Putrevu, S.K. Varma, Z. Zeng, K. Natesan, Effect of water vapor on metal dusting behavior of ferrous alloys, TMS Lett. 3 (2006) 49–50.

[23] H.Y. Yin, J. Zhang, D.J. Young, Effect of gas composition on coking and metal dusting of 2.25Cr–1Mo steel compared with iron, Corros. Sci. 51 (2009) 2983–2993.

[24] J.J. Hoffman, M. Lin, W.R. Watkins, Proposed Metal Dusting Mechanism in Lower Temperature, High Steam Syn Gas, in: Paper Presented at the Conference NACE Corrosion, Atlanta (GA), USA, March 22–26, 2009.

[25] H.J. Grabke, R. Krajak, E.M. Müller-Lorenz, S. Strauß, Metal dusting of nickel-base alloys, Mater. Corros. 47 (1996) 495–504.

[26] A. Vande Put, K.A. Unocic, M.P. Brady, B.A. Pint, Performance of Alumina-Forming Austenitic Steels, Fe-base and Ni-base Alloys Exposed to Metal Dusting Environments, in: Paper Presented at the Conference NACE Corrosion 2011, Houston (TX), USA, March 13–17, 2011.

[27] K.A. Unocic, M.P. Brady, B.A. Pint, A. Rouaix-Vande Put, Oxidation Behavior of Alumina-Forming Austenitic Steel, in: Paper Presented at the Conference NACE Corrosion, Orlando (FL), USA, March 17–21, 2013.

[28] M.P. Brady, Y. Yamamoto, M.L. Santella, B.A. Pint, Effects of minor alloy additions and oxidation temperature on protective alumina scale formation in creep-resistant austenitic stainless steels, Scripta Mater. 57 (2007) 1117–1120.

[29] Y. Yamamoto, M.P. Brady, Z.P. Lu, P.J. Maziasz, H.N. Peyer, E.A. Payzant, Creep-resistant, Al_2O_3-forming austenitic stainless steels, Science 316 (2007) 433–436.

[30] M.P. Brady, Y. Yamamoto, M.L. Santella, P.J. Maziasz, B.A. Pint, C.T. Liu, Z.P. Lu, H. Bei, The development of alumina-forming austenitic stainless steels for high-temperature structural use, JOM 60 (2008) 12–18.

[31] H.J. Grabke, Carburization, carbide formation, metal dusting, coking, Mater. Tehnol. 36 (2002) 297–305.

[32] D.J. Young, High Temperature Oxidation and Corrosion of Metals, vol. 1, Elsevier Corrosion Series, Elsevier, Cambridge (UK), 2008.

[33] A. Rouaix-Vande Put, K.A. Unocic, M.P. Brady, B.A. Pint, Performance of Al-rich alloys exposed to metal dusting environments (in preparation).

[34] V.V. Silberschmidt, E. Werner, Analysis of thermal residual stresses in duplex-type materials, Comp. Materi. Sci. 16 (1999) 39–52.

[35] H. Asteman, J.-E. Svensson, M. Norell, L.-G. Johansson, Influence of water vapor and flow rate on the high-temperature oxidation of 304L; effect of chromium oxide hydroxide evaporation, Oxid. Met. 54 (2000) 11–26.

[36] C.M. Chun, J.D. Mumford, T.A. Ramanarayanan, Mechanisms of metal dusting corrosion of iron, J. Electrochem. Soc. 149 (2002) B348–B355.

[37] P.L. Walker, J.F. Rakszawski, G.R. Imperial, Carbon formation from carbon monoxide–hydrogen mixtures over iron catalysts. 2. Rates of carbon formation, J. Phys. Chem. 63 (1959) 140–149.

[38] R. Schneider, E. Pippel, J. Woltersdorf, S. Strauss, H.J. Grabke, Microprocesses of metal dusting on nickel and Ni-base alloys, Steel Res. 68 (1997) 326–332.

[39] C.H. Toh, P.R. Munroe, D.J. Young, K. Foger, High temperature carbon corrosion in solid oxide fuel cells, Mater. High Temp. 20 (2003) 129–136.

[40] R.F. Hochman, Basic Studies of Metal Deterioration (Metal Dusting) in Carbonaceous Atmospheres at Elevated Temperatures, in: Norman E. Hamner (Ed.) (1972), Paper Presented at the 4th International Congress on Metal Corrosion, Amsterdam, The Netherlands, September 7–14, 1969, pp. 258–263.

[41] R.A. Perkins, W.C. Coons, F.J. Radd, Metal dusting corrosion in coal gasification environments, Electrochem. Soc. Inc. Proc. 77–1 (1976) 733–749.

[42] Z. Zeng, K. Natesan, M. Grimsditch, Effect of oxide scale composition on metal dusting corrosion of Fe-based alloys, Corrosion 60 (2004) 632–642.

[43] C. Anghel, E. Hörnlund, G. Hultquist, M. Limbäck, Gas phase analysis of CO interactions with solid surface at high temperatures, Appl. Surf. Sci. 233 (2004) 392–401.

[44] H.J. Grabke, Kinetics and mechanisms of surface-reactions occurring during carburization and decarburization and also nitrogenation and denitrogenation of iron in gases, Archiv Eisenhüttenwesen. 46 (1975) 75–81.

[45] H. Davies, A. Dinsdale, Theoretical study of stream grown oxides as a function of temperature, pressure and p(O2), Mater. High Temp. 22 (2005) 15–25.

[46] E. Essuman, G.H. Meier, J. Zurek, M. Hänsel, W.J. Quadakkers, The effect of water vapor on selective oxidation of Fe–Cr alloys, Oxid. Met. 69 (2008) 143–162.

[47] R. Peraldi, B.A. Pint, Effect of Cr and Ni contents on the oxidation behavior of ferritic and austenitic model alloys in air with water vapor, Oxid. Met. 61 (2004) 463–483.

[48] M.P. Brady, K.A. Unocic, M.J. Lance, M.L. Santella, Y. Yamamoto, L.R. Walker, Increasing the upper temperature oxidation limit of alumina forming austenitic stainless steels in air with water vapor, Oxid. Met. 75 (2011) 337–357.

[49] J. Zhang, P. Speck, D.J. Young, Metal dusting of alumina-forming creep-resistant austenitic stainless steels, Oxid. Met. 77 (2012) 167–187.

[50] Y. Nishiyama, K. Moriguchi, N. Otsuka, T. Kudo, Improving metal dusting resistance of transition-metals and Ni–Cu alloys, Mater. Corros. 56 (2005) 806–813.

[51] Y. Nishiyama, N. Otsuka, The role of copper in resisting metal dusting of Ni-base alloys, Mater. Sci. For. 522–523 (2006) 581–588.

[52] J. Zhang, D.J. Young, Effect of copper on metal dusting of austenitic stainless steels, Corros. Sci. 49 (2007) 1450–1467.

[53] J. Zhang, D.J. Young, Contributions of carbon permeation and graphite nucleation to the austenite dusting reaction: a study of model Fe–Ni–Cu alloys, Corros. Sci. 56 (2012) 184–193.

[54] A. Schneider, H. Viefhaus, G. Inden, H.J. Grabke, E.M. Müller-Lorenz, Influence of H2S on metal dusting, Mater. Corros. 49 (1998) 336–339.